Convection enhances mixing in the Southern Ocean

Taimoor Sohail[1,2], **Bishakhdatta Gayen**[1], **and Andrew McC. Hogg**[1,2]

[1]Research School of Earth Sciences, Australian National University, Canberra, ACT 2601, Australia
[2]ARC Centre of Excellence for Climate Extremes, Australian National University, Canberra ACT 2601, Australia

Key Points:

- We use a convection-resolving model with wind- and buoyancy-forcing to simulate an idealised Southern Ocean domain.
- Results show that local mixing efficiency has significant spatial variability.
- Turbulent convection enhances the average mixing efficiency in the Southern Ocean such that it is greater than previously assumed.

This is the author manuscript accepted for publication and has undergone full peer review but has not been through the copyediting, typesetting, pagination and proofreading process, which may lead to differences between this version and the Version of Record. Please cite this article as doi: 10.1029/2018GL077711

Corresponding author: Taimoor Sohail, taimoor.sohail@anu.edu.au

Abstract

Mixing efficiency is a measure of the energy lost to mixing compared to that lost to viscous dissipation. In a turbulent stratified fluid the mixing efficiency is often assumed constant at $\eta = 0.2$, whereas with convection it takes values closer to 1. The value of mixing efficiency when both stratified shear flow and buoyancy-driven convection are active remains uncertain. We use a series of numerical simulations to determine the mixing efficiency in an idealised Southern Ocean model. The model is energetically closed and fully resolves convection and turbulence such that mixing efficiency can be diagnosed. Mixing efficiency decreases with increasing wind stress, but are enhanced by turbulent convection and by large thermal gradients in regions with a strongly stratified thermocline. Using scaling theory and the model results, we predict an overall mixing efficiency for the Southern Ocean that is significantly greater than 0.2, while emphasising that mixing efficiency is not constant.

1 Introduction

The Southern Ocean is characterised by a meridional surface buoyancy gradient and persistent westerly winds, both of which drive circulation in this region. The surface buoyancy fluxes (both cooling and salinification) lead to the formation of dense water on the Antarctic continental shelf, which is exported as a plume of downwelling water along the continental slope and mixes to become Antarctic Bottom Water [*Kuhlbrodt et al.*, 2007; *Marshall and Speer*, 2012; *Morrison et al.*, 2015]. To balance this loss of buoyancy and maintain the stratification, turbulent diapycnal mixing transports buoyancy downwards [*Munk and Wunsch*, 1998; *Ledwell et al.*, 2000]. This turbulence is at least in part energised by surface wind stress, leading to both mixing and viscous dissipation of energy in the ocean [*Wunsch and Ferrari*, 2004]. The contribution of mixing to the total energy loss (by mixing and dissipation) is known as the mixing efficiency [*Peltier and Caulfield*, 2003]. Mixing efficiency is a fundamental quantity used to calculate the rate of overturning circulation in simple theories [*Munk and Wunsch*, 1998], interpret observations of turbulence [*Gregg*, 1989; *Alford et al.*, 1999], understand the ocean energy budget [*Wunsch and Ferrari*, 2004] and parameterise unresolved dynamics in ocean models [*Shakespeare and Hogg*, 2012].

The mixing efficiency traditionally used in oceanographic calculations has been $\eta \approx 0.2$. This value originates from experimental estimates for mixing efficiency in stratified turbulence, where mixing efficiency has a theoretical upper bound [*Linden*, 1979; *Osborn*, 1980]. However, mixing efficiency may not be a universal constant in stratified shear flows [*Peltier and Caulfield*, 2003; *Ivey et al.*, 2008]. Shear flow mixing efficiencies can be smaller than 0.2, (eg. *Prastowo et al.* [2008], *Caulfield and Peltier* [2000], *Strang and Fernando* [2001]), and the value may depend on the buoyancy Reynolds number (Re_b) and gradient Richardson number (Ri_g) [*Bouffard and Boegman*, 2013; *Mater and Venayagamoorthy*, 2014; *Salehipour et al.*, 2016]. Higher mixing efficiencies occur in stratified flows with the presence of turbulent convection. Mixing efficiencies of 0.75 in the case of Rayleigh-Taylor instability [*Davies Wykes and Dalziel*, 2014], 0.5 in the case of Rayleigh-Bénard convection [*Hughes et al.*, 2013; *Gayen et al.*, 2013a], 0.6 in the case of convectively driven instability due to internal waves [*Chalamalla and Sarkar*, 2015] and approaching 1 in the case of horizontal convection [*Gayen et al.*, 2013b, 2014; *Vreugdenhil et al.*, 2016] have been found. In addition, the presence of rough topography could enhance mixing efficiency in the abyssal ocean [*Mashayek et al.*, 2017]. It appears likely that mixing efficiency in the ocean varies substantially as a consequence of the different roles of stratification, convection, shear and wind work from place to place. The effect of turbulent convection on mixing efficiency in the context of the Southern Ocean has not been widely considered.

Numerical studies into the value of mixing efficiency for the global ocean are impeded by the inability of ocean models to fully resolve turbulent convection. High-resolution simulations which fully resolve turbulent mixing and convection have focussed on circulation regimes driven by buoyancy forcing alone, both without rotation [*Scotti and White*, 2011; *Gayen et al.*, 2013b, 2014] and with rotation [*Vreugdenhil et al.*, 2016], and leave open the question of how the results apply to the ocean. In particular, no previous simulations have resolved fully turbulent convection in concert with wind stress forcing.

In this paper we use a convection-resolving model of Southern Ocean circulation with both wind- and buoyancy-forcing to examine the local and volume-integrated diapycnal mixing, dissipation and mixing efficiency. A scaling theory is developed to predict diapycnal mixing and dissipation, and subsequently to estimate mixing efficiency in the Southern Ocean.

2 Methodology

2.1 Model Setup

An idealised re-entrant zonal channel with dimensions $H \times L \times W$ is used to represent the circumpolar Southern Ocean (figure 1). The channel is oriented such that x is Eastward, y is Northward, and z is vertically upward. The Coriolis parameter is $f(y) = f_0 + \beta y$, where $\beta = df/dy$ and $f_0 = f(y = 0)$. The simulation is forced with a hyperbolic tangent meridional distribution of surface temperature with an overall temperature difference ΔT centered about the latitude $y = W/6$ (where $T = \Delta T/2$). A steady zonal wind stress is imposed at the surface, with meridional profile $\tau(y) = \tau_{max} sin^2(4\pi y/3W)$, where τ_{max} is the maximal zonal wind stress and occurs at $y = 0.375W$ from the southern boundary. The sinusoidal lower boundary represents three Gaussian ridges (with height $h/H = 0.2$ and bathymetric contours aligned in the meridional y direction) as an idealised representation of bottom topography.

A Direct Numerical Simulation (DNS) is used to solve the incompressible, nonhydrostatic Navier-Stokes (NS) momentum equations in a rotating reference frame with a Boussinesq approximation, linear equation of state and conservation of mass and heat (see *Vreugdenhil et al.* [2016]). Planetary vorticity is assumed to be a linear function of latitude (the 'Beta-plane'). A detailed description of the NS solver and algorithm can be found in *Gayen and Sarkar* [2011] and *Gayen et al.* [2014]. The DNS are conducted using a $1024 \times 513 \times 257$ grid that is clustered to resolve the top and bottom Ekman layers and Stewartson boundary layers, and is uniform in the x-direction. All DNS solutions satisfy the standard convergence criteria (closed energy budget and fully resolved local Kolmogorov and Batchelor scales, *Gayen et al.* [2014]), which is tested for convergence across a range of high- and low-resolution simulations. A no-slip condition is applied to the side walls ($y = 0, W$) and on the bottom topography of the channel. A rigid-lid condition is imposed at the top surface of the domain ($z = H$), where a steady stress is applied for wind forcing. The end conditions at $x = 0$ and $x = L$ are periodic in the zonal direction. All boundaries are adiabatic except the top surface, where the temperature distribution is prescribed and heating and cooling occurs. The system is considered to be in thermal equilibrium when the integrated flux over the heated area is within 5% of the integrated flux over the cooled area, and fluctuations in kinetic energy are within 2% of the mean kinetic energy. All heat fluxes and mechanical energy conversions are calculated by time-averaging over at least 45 buoyancy time scales, τ_B, where $\tau_B = \sqrt{W/g'}$, and g' is reduced gravity, defined as $g' = g\alpha\Delta T$ based on the acceleration due to gravity, g and the co-efficient of thermal expansion, α.

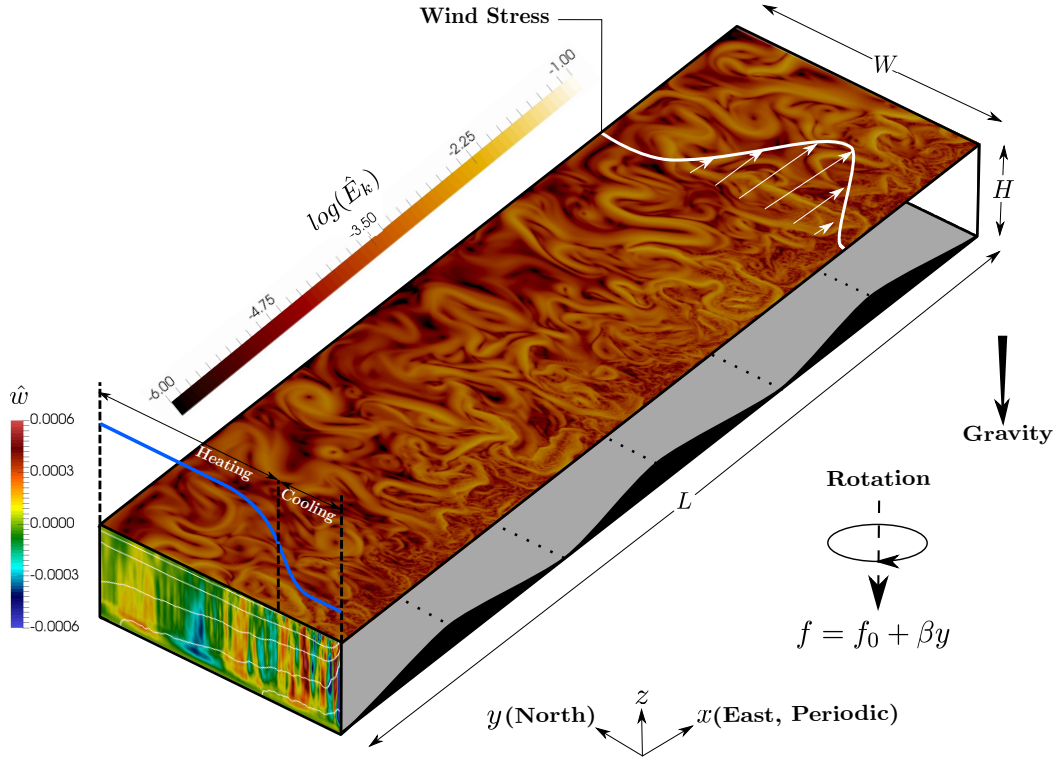

Figure 1. An overview of the model domain, with overlaid flow solution for $S = 4 \times 10^{-5}$, $Ra = 1 \times 10^{12}$ and $Ro = 4 \times 10^{-2}$. *Blue line:* Imposed surface temperature; *White line:* prescribed wind stress. On the upper horizontal plane is shown the normalised instantaneous kinetic energy, $\hat{E_k}$ inside the boundary layer at $z/H = 0.991$. The end view shows the normalised instantaneous zonally-averaged vertical velocity, $\hat{w}$, along with contours of normalised temperature, $\hat{T}$ (white), corresponding to $\hat{T} = 0.432$, 0.200, 0.189, 0.187, and 0.186 (top to bottom contours, respectively). Velocities are normalised by the scale $\sqrt{g'H}$ and temperature is expressed as $(T - T_c)/\Delta T$, where T_c is the coldest temperature.

2.2 Governing Parameters

The flow is governed by a number of non-dimensional parameters - the Rayleigh number (Ra), Ekman number (E), Prandtl number (Pr), normalised beta-plane ($\hat{\beta}$) and aspect ratios B and D:

$$Ra = \frac{g'W^3}{\nu\kappa}, E = \frac{\nu}{f_0 W^2}, Pr = \frac{\nu}{\kappa}, \hat{\beta} = \frac{\beta W}{f_0}, B = \frac{L}{W}, D = \frac{H}{W}. \quad (1)$$

Here, ν is kinematic viscosity and κ is thermal diffusivity. Molecular values of ν and κ are used for all DNS simulations. A Rossby number $Ro = U/f_0 W$ can be defined by choosing any of several velocity scales. We use $U \sim \sqrt{g'H}$, so the Rossby number can be defined in terms of external parameters as $Ro = \sqrt{g'H}/f_0 W$, leading to $Ro = (RaE^2Pr^{-1}D)^{1/2}$. In order to characterise the relative strength of wind- and buoyancy-forcing in this model, we introduce a parameter, S, which represents the ratio of the change in pressure due to imposed wind stress to that from a buoyancy differential:

$$S = \frac{\tau_{max}}{\rho_0 g' H}, \quad (2)$$

based on reference density, ρ_0.

To compare the model results with the Southern Ocean, we determine the values of the relevant non-dimensional parameters (Ra, Pr, Ro, E and S) based on observational

values of the dimensional quantities in (1). Following *Hughes et al.* [2007] and *Vreugdenhil et al.* [2016], we use estimates for turbulent viscosity and diffusivity, $\nu_T = \kappa_T = 5 \times 10^{-5} - 2 \times 10^{-4}$ m^{2}s^{-1} (50-200 times molecular values with $Pr \approx 1$) to calculate (1) for the Southern Ocean. The dimensions of the Southern Ocean are $W = 3000$ km, $H = 5$ km, and $L = 23000$ km. The maximum zonal wind stress is $\tau_{max} \approx 0.2$ Nm^{-2} [*Large and Yeager*, 2009]. The reduced gravity for the system is $g' = 0.017$, with thermal expansion co-efficient, α, estimated at an average temperature and salinity of $T = 6.7°$C and $S \approx 34$ psu to be $\alpha \sim 1 \times 10^{-4}$ C^{-1} (from TEOS-10, [*McDougall et al.*, 2009]) and $\Delta T \approx 13.4°$C [*Beggs et al.*, 2011]. Based on these values, the Rayleigh number, Ra, non-dimensional parameter, S, Ekman number, E, and Rossby number, Ro, can be estimated for the Southern Ocean, and are detailed in table 1.

Five numerical experiments with differing wind forcing (S), buoyancy forcing (Ra), and rotation (E,Ro) are conducted (table 1). In all cases, $Pr = 5$, $\hat{\beta} = 0.92$, $D = 0.4$ and $B = 5$. The aspect ratio of the channel, D, is selected to ensure the thermal boundary layer thickness, δ_T is smaller than domain height ($\delta_T \ll H$) for the range of Ra in this study, where simulated δ_T is calculated as the e-folding distance from the heated top surface. We achieve O(10) Rossby deformation radii across the channel width, and the DNS replicates a large ($\sim 10^4$) scale separation between the turbulent Kolmogorov scale and the basin scale (channel width). The simulations are conducted at the highest Rayleigh number possible given modern computational resources, but aspect ratio is greater than that of the Southern Ocean, reducing the scale separation of the Rossby radius and convective vortices.

Case	Ra	S	E	Ro
A	1.125×10^{12}	0	4×10^{-7}	0.12
B	1.125×10^{12}	4.44×10^{-5}	4×10^{-7}	0.12
C	1.125×10^{12}	8.89×10^{-5}	4×10^{-7}	0.12
D	1.125×10^{12}	1.77×10^{-4}	4×10^{-7}	0.12
E	3.75×10^{10}	1.33×10^{-3}	2×10^{-6}	0.11
SO	$1.2 \times 10^{25} - 1.9 \times 10^{26}$	2.3×10^{-6}	$4.44 \times 10^{-14} - 1.78 \times 10^{-13}$	0.025

Table 1. The relevant non-dimensional parameters for the suite of simulations conducted (A-E). Case SO represents the non-dimensional parameters for the Southern Ocean, calculated from observational values.

2.3 Energetic Framework

Local diapycnal mixing is:

$$\Phi_d = -\kappa g \left(\frac{\partial z^*}{\partial \rho}\right)\left(\frac{\partial \rho}{\partial x_j}\right)^2, \tag{3}$$

where z^* is the height above the base at which each water parcel would be found when the fluid was adiabatically resorted to a statically stable state, as done here [*Winters et al.*, 1995]. Local viscous dissipation is defined as the spatial gradient of the total instantaneous velocity:

$$\varepsilon = \rho_0 \nu (\partial u_i / \partial x_j)^2. \tag{4}$$

The individual terms in the energy budget are normalised by the domain averaged rate of potential energy generation from internal energy:

$$\Phi_i = \kappa g A \overline{\rho}_{top} - \kappa g \int\int \rho(x, y, h(x, y)) dx dy \tag{5}$$

where A is the area of the top surface of the domain, $\overline{\rho}_{top}$ is the average density at the top surface and $\rho(x, y, h(x, y))$ is the bottom density along the topography. The average mixing efficiency is defined as the ratio of diapycnal mixing to the total mechanical energy sink, expressed mathematically as [*Peltier and Caulfield*, 2003]:

$$\eta = \frac{\langle \Phi_d \rangle - \langle \Phi_i \rangle}{\langle \Phi_d \rangle - \langle \Phi_i \rangle + \langle \varepsilon \rangle}, \tag{6}$$

where the angled brackets indicate a volume integral. While other definitions of mixing efficiency exist (see *Osborn* [1980]; *Ivey and Imberger* [1991]), we adopt (6) because it is unaffected by the large reversible energy fluxes in buoyancy-dominated flows such as convection.

We also define a local mixing efficiency, $\eta_L = \Phi_d/(\Phi_d + \varepsilon)$; this definition differs from (6) as it omits Φ_i to ensure that η_L cannot exceed 1. The terms in (6) are volume-integrated, hence the volume-averaged η_L will not equal to average mixing efficiency, η, i.e., $\frac{1}{V}\int \eta_L dV \neq \eta$.

3 Results

The thermally equilibrated model exhibits a wide range of scales of motion, from small-scale convection to geostrophic flow (figure 1) with a vertical stratification (white lines show isopycnals on the $y - z$ plane in figure 1). Wind stress and surface buoyancy fluxes combine to steepen the ispoycnals, which excites baroclinic eddies, and subsequently flattens the isopycnals [*Karsten et al.*, 2002]. These eddies can be seen in the kinetic energy plot on the top surface of the domain (figure 1), and are also present in the zonally-averaged view as regions of transient upwelling and downwelling (see online multimedia). The stratification also results in the formation of a braided, meandering zonal jet along the channel through thermal wind balance [*Hogg*, 2010]. Small-scale vertical convection is present in the region of destabilising buoyancy, with a persistent downwelling plume present along the southern boundary (vertical velocity in figure 1). Thus, the model exhibits many of the observed characteristics of flow in the Southern Ocean.

There is spatial variation of both local dissipation and diapycnal mixing (figure 2a-d). Largest dissipation rates are observed inside the top boundary layer and are concentrated in the horizontal band of applied wind stress which spans $3/4$ of the channel width (figure 2a,b). The fronts associated with zonal jets and baroclinic eddies are regions of high dissipation [*Barkan et al.*, 2015]. Dissipation is also large in the turbulent convective plume. Dissipation is low in the interior away from the convective zone and the stably stratified boundary layer. Diapycnal mixing is similarly concentrated in regions of active convection and inside the top boundary layer (figure 2c, d), as a result of the large near-surface stratification, which is enhanced due to shear associated with the mean flow.

Local mixing efficiency, η_L, varies significantly over the domain (figure 2e-f). η_L is high where convection is dominant and in the stably stratified boundary layer region, where diapycnal mixing is large. Dissipation is enhanced by surface wind stress, leading to smaller local mixing efficiency in the thin boundary layer underlying the horizontal band of wind stress (not visible in the figure). The variation of both diapycnal mixing and dissipation rate with depth is qualitatively similar. However, diapycnal mixing is smaller than dissipation throughout the interior, giving $\eta_L < 0.5$ in the interior (zonally averaged). Mixing is greater than dissipation in the upper 25% of the domain, giving $\eta_L > 0.5$, and η_L approaches 1 in the northern 30% of the domain.

Figure 3a shows the change in normalised, time-averaged and volume-integrated diapycnal mixing, $\langle \widehat{\Phi}_d \rangle$, and viscous dissipation rate, $\langle \widehat{\varepsilon} \rangle$ with wind stress. Dissipation increases with increased wind stress because the majority of momentum imparted by the wind stress is dissipated very close to the surface of the model. At small wind stress the

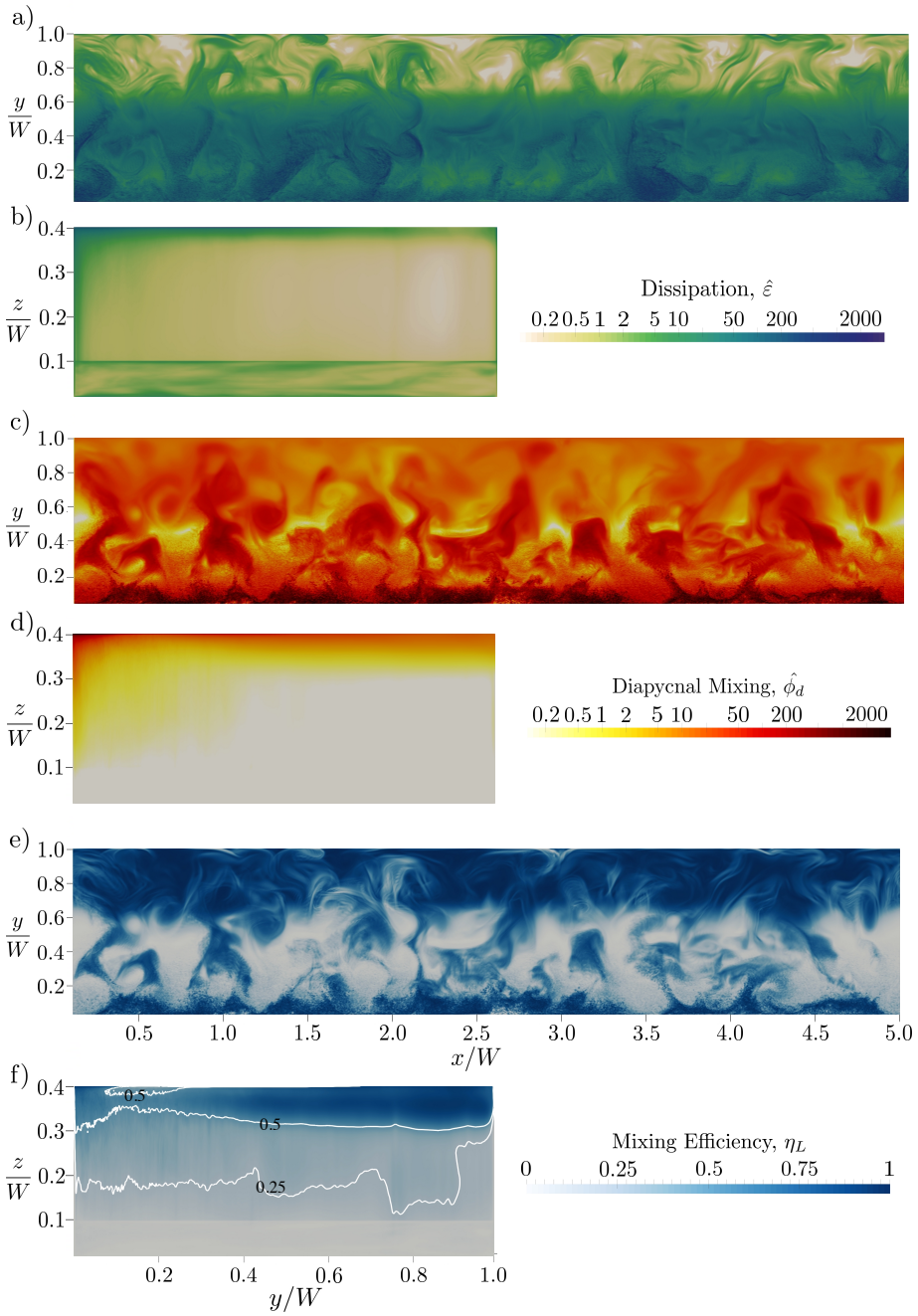

Figure 2. Time-averaged spatial distribution of energetics terms for case D: a) top surface and b) zonally-averaged dissipation, $\widehat{\varepsilon}$; c) top surface and d) zonally-averaged diapycnal mixing, $\widehat{\Phi}_d$; and e) top surface and f) zonally-averaged local mixing efficiency, η_L. The top surface plots are at a depth of $z/W = 0.398$, within the thermal boundary layer. Energetics are normalised by Φ_i. Contour lines in (f) show mixing efficiency of 0.5 and 0.25.

dissipation approaches the theoretical limit, $\langle\varepsilon\rangle \rightarrow \langle\Phi_i\rangle$ (represented by case A) as noted by *Paparella and Young* [2002]. Diapycnal mixing also increases with increasing wind stress. Increasing the imposed wind stress steepens the isopycnals, thereby increasing the surface buoyancy uptake and consequently increasing diapycnal mixing (which is dependent only on buoyancy uptake, *Hughes et al.* [2013]). This indirect coupling between wind

stress and mixing is highlighted by ocean model results [*Saenz et al.*, 2012]. The absolute value of diapycnal mixing is greater than the changes of mixing with wind stress, implying that buoyancy forcing is the dominant driver of diapycnal mixing within the range of conditions studied here.

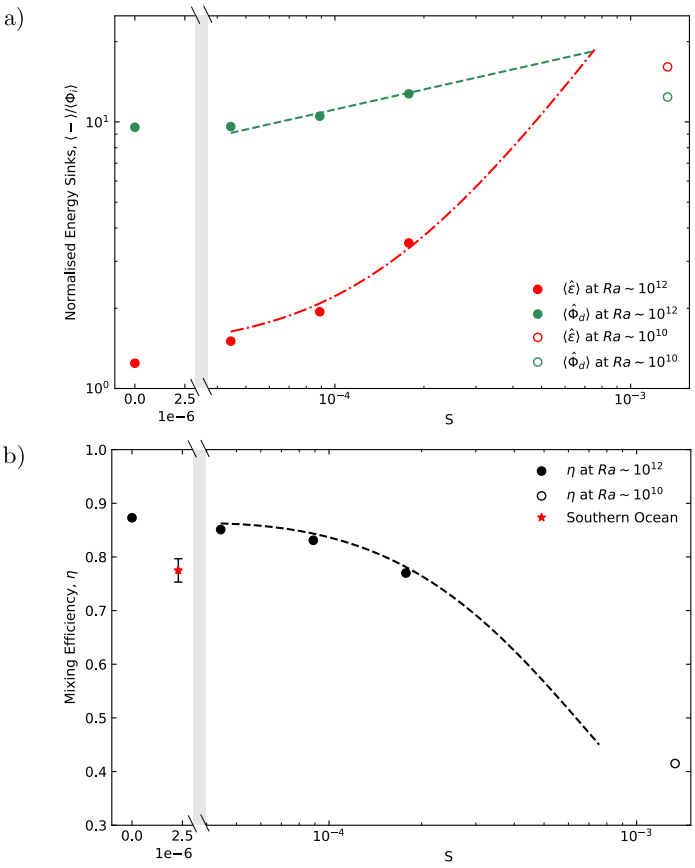

Figure 3. a) The time-averaged, volume-integrated normalised dissipation, $\langle\widehat{\varepsilon}\rangle$ and diapycnal mixing, $\langle\widehat{\Phi_d}\rangle$ as functions of the relative wind stress, S, and b) variation of mixing efficiency, η, with the relative wind stress S. *Filled Circles*: cases A - D; *Open Circle*: case E. The energetics are normalised by $\langle\Phi_i\rangle$. Lines are the predictions of the scaling theory.

Mixing efficiency, calculated from equation (6), is shown in figure 3b as a function of S. The mixing efficiency is large, $0.8 < \eta < 0.9$, in cases A - D. Case E (open circle) lies in the laminar boundary layer regime (identified by *Gayen et al.* [2013b] as $Ra < 10^{11}$), and consequently has a reduced mixing efficiency (consistent with *Barkan et al.* [2013]). This result suggests that turbulent convection enhances diapycnal mixing and mixing efficiency. At small wind stress mixing efficiency is asymptotic to the theoretical value given by (6) with $\langle\varepsilon\rangle = \langle\Phi_i\rangle$, so $\eta = 1 - \langle\Phi_i\rangle/\langle\Phi_d\rangle$ as shown in previous horizontal convection studies [*Vreugdenhil et al.*, 2016]. When mixing efficiency is calculated with turbulent, instead of total, dissipation in (6), it does not vary significantly.

4 Application to Ocean

To apply the model results to the Southern Ocean (where Rayleigh number is higher and aspect ratio smaller), scaling theories are needed. In thermal equilibrium the diapyc-

nal mixing rate is given by $\langle \Phi_d \rangle = \langle \Phi_{b2} \rangle$ [*Hughes et al.*, 2009], where $\langle \Phi_{b2} \rangle$ is the mechanical power input by surface buoyancy fluxes, defined as:

$$\langle \Phi_{b2} \rangle = -\kappa g \oint z^* (\partial \rho / \partial x_i) dA, \tag{7}$$

where A is the top surface of the domain. Viscous dissipation equates to the sum of the background rate of molecular diffusion and the kinetic energy input by surface wind stress into the system:

$$\langle \varepsilon \rangle = \langle \Phi_\tau \rangle + \langle \Phi_i \rangle, \tag{8}$$

where $\langle \Phi_\tau \rangle$ is wind work, expressed as:

$$\langle \Phi_\tau \rangle = \oint \tau u \big|_{z=H} dA, \tag{9}$$

and $u\big|_{z=H}$ is velocity at the top surface. Therefore, if the power inputs by buoyancy and wind work are known, the diapycnal mixing and viscous dissipation rates can be predicted.

In thermal equilibrium the net heat flux through every horizontal level of the domain is zero. Therefore, the buoyancy uptake can be estimated from the thickness, δ, of the stably stratified region of the thermal boundary layer. With surface buoyancy forcing alone a horizontal thermal wind balance and vertical advection-diffusion balance is established and the thermal boundary layer thickness can consequently be expressed as $\delta \sim (\kappa f_0 W^2 / g')^{1/3}$ [*Robinson and Stommel*, 1959; *Welander*, 1971; *Winton*, 1996; *Park and Bryan*, 2000; *Vreugdenhil et al.*, 2016]. When wind stress is introduced, the vertical advection near the surface is dominated by Ekman pumping with vertical velocity $w_E \sim \tau_{max}/(\rho_0 f_0 W)$, resulting in a "modified" thermal boundary layer thickness of $\delta_T \sim [\rho_0 f_0^2 \kappa^2 W^3 / (g' \tau_{max})]^{1/4}$ [see derivation in *Samelson and Vallis*, 1997]. δ_T can be expressed in terms of non-dimensional parameters as:

$$\delta_T / W = c_{\delta_T} (SRo^2 RaPr)^{-1/4}, \tag{10}$$

where the value of the prefactor $c_{\delta_T} = 0.70$ can be determined from simulations.

The power input by buoyancy, $\langle \Phi_{b2} \rangle$, is defined in terms of the resorted height, z^*. We find that $z^* \approx H$ in the heated region of the domain (where less dense water parcels exist) and $z^* \approx 0$ in the cooled section (where more dense water parcels are present). Hence, the diapycnal mixing can be approximated by $\langle \Phi_d \rangle = \langle \Phi_{b2} \rangle \approx \kappa \rho_0 g \alpha a_h H \overline{dT/dz}\Big|_h \sim \kappa \rho_0 g \alpha a_h H (\Delta T / \delta_T)$, where the subscript h indicates the heated region and $\overline{dT/dz}\Big|_h$ is the spatially averaged vertical temperature gradient at the boundary in the heated region, which has area a_h. The normalised diapycnal mixing is then:

$$\langle \widehat{\Phi}_d \rangle = \frac{\langle \Phi_d \rangle}{\langle \Phi_i \rangle} \sim \frac{H}{\delta_T} \sim (SRo^2 PrRaD^4)^{1/4}, \tag{11}$$

where the rate of generation of potential energy is $\langle \Phi_i \rangle \approx \kappa \rho_0 g \alpha \Delta T a_h$.

To predict viscous dissipation, we first estimate the wind work, which scales as $\langle \Phi_\tau \rangle \sim u_a \tau_{max} W L$. We assume that ageostrophic motion dominates surface zonal flow when wind forcing is sufficiently high. Therefore, the velocity in (9) is u_a, the ageostrophic zonal velocity scale. From Ekman layer theory [*Ekman*, 1905], the ageostrophic surface zonal flow is $u_a \sim \tau_{max}/(\rho_0 f_0 \delta_E)$, where δ_E is the turbulent Ekman layer thickness, $\delta_E = 0.5\sqrt{\tau_{max}/\rho_0}/f_0$ [*Coleman et al.*, 1990; *Price and Sundermeyer*, 1999; *Wang and Huang*, 2004]. The normalised wind work becomes:

$$\langle \widehat{\Phi}_\tau \rangle = \frac{\langle \Phi_\tau \rangle}{\langle \Phi_i \rangle} \sim (S^3 RaPrD^3)^{1/2}. \tag{12}$$

From (8), the normalised viscous dissipation rate at thermal equilibrium is estimated as:

$$\langle \widehat{\varepsilon} \rangle = \frac{\langle \varepsilon \rangle}{\langle \Phi_i \rangle} \sim 1 + (S^3 RaPrD^3)^{1/2}. \tag{13}$$

The scaling for diapycnal mixing (11) and dissipation (13) is tested against the computed flow solutions in figure 3a. Both quantities follow the scaling predictions closely. The average mixing efficiency predicted by (6) is shown in figure 3b and the theoretical estimation is in good agreement with the DNS. However, the scaling theory does not provide a good prediction for case E because this simulation lies outside the turbulent convective regime ($Ra > 10^{11}$; *Gayen et al.* [2014]).

From the scaling and ocean variables given in section 2.2, we determine that the thermal boundary layer thickness for the Southern Ocean is $\delta_T \approx [200 - 400]$ m. The rate of conversion from internal to potential energy is estimated to lie in the range $\langle \Phi_i \rangle = [0.04 - 0.2]$ TW, with a_h assumed to be 70% of the surface area of the Southern Ocean. The scaling gives a diapycnal mixing rate $\langle \Phi_d \rangle \approx [0.9 - 2]$ TW. The wind work is predicted to be $\langle \Phi_\tau \rangle \approx 0.22$ TW, which is close to inferences from observations [*Wunsch*, 1998; *Hughes and Wilson*, 2008; *Roquet et al.*, 2011]. From (13), we estimate that dissipation is $\langle \varepsilon \rangle \approx [0.3 - 0.4]$ TW. From (6) we predict an average mixing efficiency $\eta \approx [0.75 - 0.80]$ for the Southern Ocean.

5 Discussion & Conclusions

Energetically closed, turbulence-resolving solutions with wind- and buoyancy-forcing are used to investigate the impact of convection on diapycnal mixing and turbulent dissipation in our model of the Southern Ocean. Local dissipation is highest near the surface of the domain underlying wind stress forcing, and in the regions of deep convection, whereas local diapycnal mixing is highest in regions of turbulent convection, as well as in the stably stratified region in the northern half of the domain. Therefore, highest values of local mixing efficiency are observed inside the deep convection region and in the buoyancy stabilising region, where a strong vertical buoyancy gradient is present. Overall, small-scale convection enhances volume-integrated diapycnal mixing to be greater than dissipation so that mixing efficiency is in the range $\eta \approx 0.8 - 0.9$ within oceanographically realistic values of S. Increasing wind stress enhances both volume-integrated dissipation and diapycnal mixing, but ultimately reduces mixing efficiency. Using a scaling analysis which matches the DNS results, we predict that mixing efficiency in the Southern Ocean might have a value of as high as $\eta \approx 0.78$. These findings indicate that convection increases mixing efficiency and the results cast doubt on assumptions that mixing efficiency is uniform and is controlled solely by shear-driven instabilities. In addition, the spatial variance of mixing efficiency indicates regions where the majority of energy loss goes to mixing. This information may be used in targeted observational studies of mixing in the future.

We have focussed here on the role of wind and buoyancy forcing on dissipation and diapycnal mixing. However, tides have been predicted to introduce up to 3.7 TW of mechanical energy into the global ocean. Approximately $0.6 - 0.9$ TW of this tidal energy may contribute to diapycnal mixing [*Munk and Wunsch*, 1998]. Further studies with a turbulence-resolving model incorporating tidal mixing would be useful in elucidating the impact of tidal forcing on the mechanical energy budget of the Southern Ocean. There is also a significant difference between the aspect ratios used in the present model and those in the ocean. While this difference is taken into account in the theoretical scaling analysis used here to predict the energetics of the Southern Ocean, the accuracy of the aspect ratio dependence has not been tested in the DNS.

Acknowledgments

Numerical simulations were conducted on the Australian National Computational Infrastructure (NCI), ANU, which is supported by the Commonwealth of Australia. This research was supported by the Australian Research Council (ARC) grant DP140103706. T.S. was supported by the Endeavour Scholarships and Fellowships 5256_2016, and B.G. by an ARC DECRA Fellowship DE140100089 and the R. J. L. Hawke Fellowship. We are grateful for the advice and direction provided by C. A. Vreugdenhil, R. W. Griffiths and K. D. Stewart in earlier versions of this paper. Model outputs are available in the supplementary data.

References

Alford, M. H., M. C. Gregg, and M. Ilyas (1999), Diapycnal mixing in the Banda Sea: Results of the first microstructure measurements in the Indonesian throughflow, *Geophysical Research Letters*, *26*(17), 2741–2744.

Barkan, R., K. B. Winters, and S. G. L. Smith (2013), Rotating horizontal convection, *J. Fluid Mech.*, *723*, 556–586.

Barkan, R., K. B. Winters, and S. G. L. Smith (2015), Energy cascades and loss of balance in a reentrant channel forced by wind stress and buoyancy fluxes, *Journal of Physical Oceanography*, *45*, 272–293.

Beggs, H., A. Zhong, G. Warren, O. Alves, G. Brassington, and T. Pugh (2011), RAMSSA - an operational, high-resolution, regional Australian multi-sensor sea surface temperature analysis over the Australian region, *Australian Meteorological and Oceanographic Journal*, *61*, 1–22.

Bouffard, D., and L. Boegman (2013), A diapycnal diffusivity model for stratified environmental flows, *Dynamics of Atmospheres and Oceans*, *61*, 14–34.

Caulfield, C. P., and W. R. Peltier (2000), The anatomy of the mixing transition in homogeneous and stratified free shear layers, *Journal of Fluid Mechanics*, *413*, 1–47.

Chalamalla, V. K., and S. Sarkar (2015), Mixing, dissipation rate, and their overturn-based estimates in a near-bottom turbulent flow driven by internal tides, *Journal of Physical Oceanography*, *45*(1969-1987).

Coleman, G. N., J. H. Ferzinger, and P. Spalart (1990), A numerical study of the turbulent Ekman layer, *Journal of Fluid Mechanics*, *213*, 313–348.

Davies Wykes, M., and S. Dalziel (2014), Efficient mixing in stratified flows: Experimental study of a Rayleigh–Taylor unstable interface within an otherwise stable stratification., *Journal of Fluid Mechanics*, *756*, 1027–1057.

Ekman, V. W. (1905), On the influence of the Earth's rotation on ocean currents, *Archives of Mathematics, Astronomy and Physics*, *2*, 1–52.

Gayen, B., and S. Sarkar (2011), Direct and large-eddy simulations of internal tide generation at a near-critical slope, *Journal of Fluid Mechanics*, *681*(48-79).

Gayen, B., G. O. Hughes, and R. W. Griffiths (2013a), Completing the mechanical energy pathways in turbulent Rayleigh-Bénard convection, *Physical Review Letters*, *111*(124301), 1–5.

Gayen, B., R. W. Griffiths, G. O. Hughes, and J. A. Saenz (2013b), Energetics of horizontal convection, *Journal of Fluid Mechanics*, *716*(R10), 1–11.

Gayen, B., R. W. Griffiths, and G. O. Hughes (2014), Stability transitions and turbulence in horizontal convection, *Journal of Fluid Mechanics*, *751*, 698–724.

Gregg, M. C. (1989), Scaling turbulent dissipation in the thermocline, *Journal of Geophysical Research*, *94*(C7), 9686–9698.

Hogg, A. M. (2010), An Antarctic Circumpolar Current driven by surface buoyancy forcing, *Geophysical Research Letters*, *37*.

Hughes, C. W., and C. Wilson (2008), Wind work on the geostrophic ocean circulation: An observational study of the effect of small scales in the wind stress, *Journal of Geophysical Research*, *113*(C02016), 1–10.

Hughes, G. O., R. W. Griffiths, J. C. Mullarney, and W. H. Peterson (2007), A theoretical model for horizontal convection at high Rayleigh number, *Journal of Fluid Mechanics*, *581*, 251–276.

Hughes, G. O., A. M. Hogg, and R. W. Griffiths (2009), Available potential energy and irreversible mixing in the meridional overturning circulation, *Journal of Physical Oceanography*, *39*, 3130–3146.

Hughes, G. O., B. Gayen, and R. W. Griffiths (2013), Available potential energy in Rayleigh-Bénard convection, *Journal of Fluid Mechanics*, *729*.

Ivey, G. N., and J. Imberger (1991), On the nature of turbulence in a stratified fluid. part i: The energetics of mixing, *Journal of Physical Oceanography*, *21*, 650 – 658.

Ivey, G. N., K. B. Winters, and J. R. Koseff (2008), Density stratification, turbulence, but how much mixing?, *Annual Review of Fluid Mechanics*, *40*, 169–184.

Karsten, R., H. Jones, and J. Marshall (2002), The role of eddy transfer in setting the stratification and transport of a circumpolar current, *Journal of Physical Oceanography*, *32*, 39–54.

Kuhlbrodt, T., A. Griesel, M. Montoya, A. Levermann, M. Hofmann, and S. Rahmstorf (2007), On the driving processes of the Atlantic Meridional Overturning Circulation, *Reviews of Geophysics*, *45*(2004RG000166), 1–32.

Large, W. G., and S. G. Yeager (2009), The global climatology of an interannually varying air–sea flux data set., *Climate Dynamics*, *33*(2-3), 341–364.

Ledwell, J. R., E. T. Montgomery, K. L. Polzin, L. C. S. Laurent, R. W. Schmitt, and J. M. Toole (2000), Evidence for enhanced mixing over rough topography in the abyssal ocean, *Nature*, *403*, 179–182.

Linden, P. F. (1979), Mixing in stratified fluids, *Geophysical and Astrophysical Fluid Dynamics*, *13*(1), 3–23.

Marshall, J., and K. Speer (2012), Closure of the meridional overturning circulation through Southern Ocean upwelling, *Nature Geoscience*, *5*, 171–180.

Mashayek, A., H. Salehipour, D. Bouffard, C. P. Caulfield, R. Ferrari, M. Nikurashin, W. R. Peltier, and W. D. Smyth (2017), Efficiency of turbulent mixing in the abyssal ocean circulation, *Geophysical Research Letters*, *44*, 6296–6306.

Mater, B. D., and S. K. Venayagamoorthy (2014), A unifying framework for parameterizing stably stratified shear-flow turbulence, *Physics of Fluids*, *26*(036601).

McDougall, T. J., R. Feistel, F. J. Millero, D. R. Jackett, D. G. Wright, B. A. King, G. M. Marion, C.-T. A. Chen, P. Spitzer, and S. Seitz (2009), The international thermodynamic equation of seawater 2010 (TEOS-10): Calculation and use of thermodynamic properties, *Global Ship-based Repeat Hydrography Manual, IOCCP Report No*, *14*.

Morrison, A. K., T. L. Frolicher, and J. L. Sarmiento (2015), Upwelling in the Southern Ocean, *Physics Today*, pp. 27–32.

Munk, W. H., and C. Wunsch (1998), Abyssal recipes II: energetics of tidal and wind mixing, *Deep Sea Research I*, *45*, 1977–2010.

Osborn, T. R. (1980), Estimates of the local rate of vertical diffusion from dissipation measurements, *Journal of Physical Oceanography*, *10*, 83–89.

Paparella, F., and W. R. Young (2002), Horizontal convection is non-turbulent, *Journal of Geophysical Research*, *466*, 205–214.

Park, Y.-G., and K. Bryan (2000), Comparison of thermally driven circulations from a depth-coordinate model and an isopycnal-layer model. part I: Scaling-law sensitivity to vertical diffusivity, *Journal of Physical Oceanography*, *30*, 590–605.

Peltier, W. R., and C. P. Caulfield (2003), Mixing efficiency in stratified shear flows, *Annual Review of Fluid Mechanics*, *15*, 135–167.

Prastowo, T., R. W. Griffiths, G. O. Hughes, and A. M. Hogg (2008), Mixing efficiency in controlled exchange flows, *Journal of Fluid Mechanics*, *600*, 235–244.

Price, J. F., and M. A. Sundermeyer (1999), Stratified Ekman layers, *Journal of Geophysical Research*, *104*(C9), 20,467–20,494.

Robinson, A., and H. Stommel (1959), The oceanic thermocline and the associated thermohaline circulation, *Tellus*, *11*(3), 295–308.

Roquet, F., C. Wunsch, and G. Madec (2011), On the patterns of wind-power input to the ocean circulation, *Journal of Physical Oceanography*, *41*, 2328–2342.

Saenz, J. A., A. M. Hogg, G. O. Hughes, and R. W. Griffiths (2012), Mechanical power input from buoyancy and wind to the circulation in an ocean model, *Geophysical Research Letters*, *39*(L13605), 1–6.

Salehipour, H., W. R. Peltier, C. B. Whalen, and J. A. MacKinnon (2016), A new characterization of the turbulent diapycnal diffusivities of mass and momentum in the ocean, *Geophysical Research Letters*, *43*, 3370–3379.

Samelson, R. M., and G. K. Vallis (1997), Large-scale circulation with small diapycnal diffusion: The two-thermocline limit, *Journal of Marine Research*, *55*, 223–275.

Scotti, A., and B. White (2011), Is horizontal convection really "non-turbulent?", *Geophysical Research Letters*, *38*, L21,609.

Shakespeare, C. J., and A. M. Hogg (2012), An analytical model of the response of the meridional overturning circulation to changes in wind and buoyancy forcing, *Journal of Physical Oceanography*, *42*, 1270–1287.

Strang, E. J., and H. J. S. Fernando (2001), Entrainment and mixing in stratified shear flows, *Journal of Fluid Mechanics*, *428*, 349 – 386.

Vreugdenhil, C. A., B. Gayen, and R. W. Griffiths (2016), Mixing and dissipation in a geostrophic buoyancy-driven circulation, *Journal of Geophysical Research: Oceans*, *121*, 6076–6091.

Wang, W., and R. X. Huang (2004), Wind energy input to the Ekman layer, *Journal of Physical Oceanography*, *34*, 1267–1275.

Welander, P. (1971), The thermocline problem, *Philosophical Transactions of the Royal Society of London*, *270*, 415–421.

Winters, K. B., P. N. Lombard, J. J. Riley, and E. A. D'Asaro (1995), Available potential energy and mixing in density-stratified fluids, *Journal of Fluid Mechanics*, *289*, 115–128.

Winton, M. (1996), The role of horizontal boundaries in parameter sensitivity and decadal-scale variability of coarse-resolution ocean general circulation models, *Journal of Physical Oceanography*, *26*(3), 289–304.

Wunsch, C. (1998), The work done by the wind on the oceanic general circulation, *Journal of Physical Oceanography*, *28*, 2332–2340.

Wunsch, C., and R. Ferrari (2004), Vertical mixing, energy, and the general circulation of the oceans, *Annual Review of Fluid Mechanics*, *36*, 281–314.

Figure 1.

Wind Stress

W

H

$log(\hat{E}_K)$

-1.00

-2.25

-3.50

-4.75

-6.00

$\hat{w}$

0.0006

0.0003

0.0000

-0.0003

-0.0006

Heating

Cooling

L

Gravity

Rotation

$f = f_0 + \beta y$

y**(North)**

z

x**(East, Periodic)**

Figure 2.

a)

b)

c)

d)

e)

f)

y/W

z/W

x/W

Dissipation, $\hat{\varepsilon}$

0.2 0.5 1 2 5 10 50 200 2000

Diapycnal Mixing, $\hat{\phi}_d$

0.2 0.5 1 2 5 10 50 200 2000

Mixing Efficiency, η_L

0 0.25 0.5 0.75 1

Figure 3.

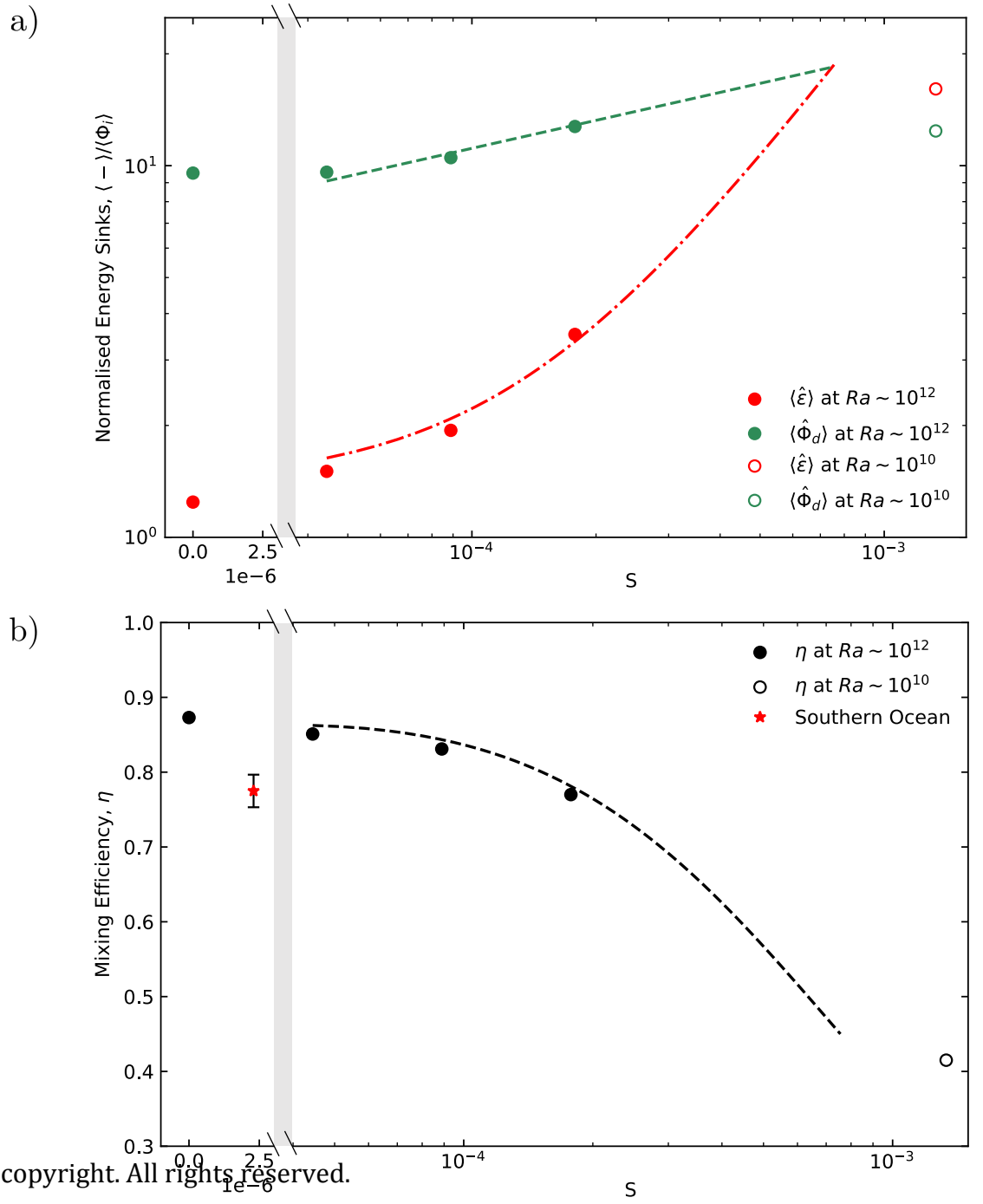

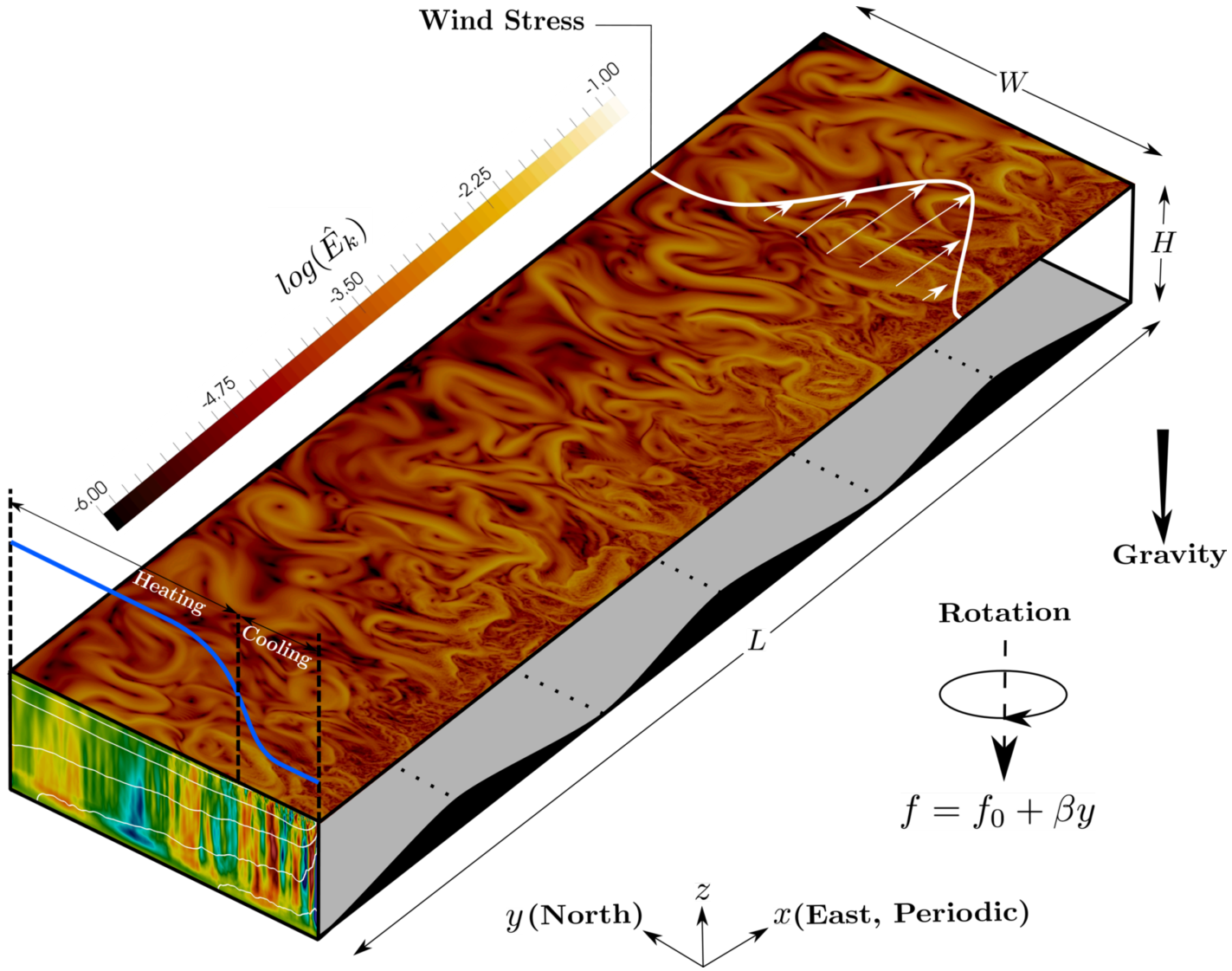

2018gl077711-f01-z-.eps

a)

b)

c)

d)

e)

f)

y/W

z/W

x/W

Dissipation, $\hat{\varepsilon}$

0.2 0.5 1 2 5 10 50 200 2000

Diapycnal Mixing, $\hat{\phi}_d$

0.2 0.5 1 2 5 10 50 200 2000

Mixing Efficiency, η_L

0 0.25 0.5 0.75 1